aerospace

MDPI

Article

Coupled Fluid–Solid Numerical Simulation for Flow Field Characteristics and Supporting Performance of Flexible Support Cylindrical Gas Film Seal

Junfeng Sun [1], Meihong Liu [1,*], Zhen Xu [2], Taohong Liao [3], Xiangping Hu [4,*], Yuxian Li [1] and Juan Wang [1]

[1] Faculty of Mechanical and Electrical Engineering, Kunming University of Science and Technology, Kunming 650504, China; junfengsun@139.com (J.S.); yuxian@kust.edu.cn (Y.L.); wjjy_0908@126.com (J.W.)
[2] Faculty of Mechanical and Electrical Engineering, Yunnan Open University, Kunming 650500, China; xuzhen108@126.com
[3] Department of Marine Technology, Norwegian University of Science and Technology, NO-7491 Trondheim, Norway; liao.taohong@gmail.com
[4] Industrial Ecology Programme, Department of Energy and Process Engineering, Norwegian University of Science and Technology, NO-7491 Trondheim, Norway
* Correspondence: 13648861980@163.com (M.L.); Xiangping.Hu@ntnu.no (X.H.)

Abstract: A new type of cylindrical gas film seal (CGFS) with a flexible support is proposed according to the working characteristics of the fluid dynamic seal in high-rotational-speed fluid machinery, such as aero-engines and centrifuges. Compared with the CGFS without a flexible support, the CGFS with flexible support presents stronger radial floating characteristics since it absorbs vibration and reduces thermal deformation of the rotor system. Combined with the structural characteristics of a film seal, an analytical model of CGFS with a flexible wave foil is established. Based on the fluid-structure coupling analysis method, the three-dimensional flow field of a straight-groove CGFS model is simulated to study the effects of operating and structural parameters on the steady-state characteristics and the effects of gas film thickness, eccentricity, and the number of wave foils on the equivalent stress of the flexible support. Simulation results show that the film stiffness increases significantly when the depth of groove increases. When the gas film thickness increases, the average equivalent stress of the flexible support first decreases and then stabilizes. Furthermore, the number of wave foils affects the average foils thickness. Therefore, when selecting the number of wave foils, the support stiffness and buffer capacity should be considered simultaneously.

Keywords: cylindrical gas film seal; flexible support performance; operating parameters; structural parameters; fluid-structure coupling

Citation: Sun, J.; Liu, M.; Xu, Z.; Liao, T.; Hu, X.; Li, Y.; Wang, J. Coupled Fluid–Solid Numerical Simulation for Flow Field Characteristics and Supporting Performance of Flexible Support Cylindrical Gas Film Seal. *Aerospace* **2021**, *8*, 97. https://doi.org/10.3390/aerospace8040097

Academic Editor: Erinc Erdem

Received: 19 February 2021
Accepted: 30 March 2021
Published: 2 April 2021

1. Introduction

The development of the modern aviation engine has reached a high level, but the structural design cost of the compressor and the turbine of an aviation engine is increasing exponentially. In comparison with improving the engine's sealing performance by enhancing its structure, advanced sealing technology can reduce the engine's fuel consumption and leakage while improving its efficiency at a lower cost [1]. The results of NASA's advanced subsonic technology program show that the advanced gas film-sealing technology can improve the sealing performance, reduce leakage, and prolong the operating life of the engine in a harsh working environment. The advanced sealing technology also plays an important role in reducing the fuel consumption rate and the cost of the engine [2–4]. As an advanced non-contact sealing technology, cylindrical gas film seal (CGFS) has several advantages, such as low leakage and energy consumption, long serving life, high reliability, and floating adaptability [5–7], and the CGFS can even be used in the so-called three-high working conditions (high interface sliding speed, high boundary pressure difference, high ambient temperature) with large dynamic displacement of the rotor (caused by severe

vibration and thermal deformation) [8,9]. Therefore, it is worthwhile to conduct research on the flexible-support CGFS.

The CGFS system mainly consists of flexible wave foils and floating rings, and its flexible support of the rotor allows a large radial displacement in operation [10]. In this system, the film thickness is usually very thin, i.e., a few micrometers, but the radial vibration of the shaft can reach several millimeters. To avoid sealing failure caused by contact between shaft and sealing surface of the floating ring, its structural parameters should be selected carefully. Ma et al. have carried out investigation on the dynamic-state and steady-state characteristics of CGFS. They found out the rules between the sealing performance and the compressible number and film thickness. They also obtained the formulas for the dynamic stiffness factor and damping coefficient, and they claimed that their results provide a theoretical basis for the establishment of accurate gas film model [11–13]. Chen et al. established the T-groove model and no-groove model and analyzed the impact of operation parameters on the sealing ability of the two models. Their results showed that the T-groove structure has a better hydrodynamic effect than the non-groove model. These results provide theoretical support for the selection of reasonable fluid dynamic pressure groove [6]. Ding et al. proposed a new floating cylindrical micro groove gas film seal model, studied the impact of surface micro pits and micro grooves on the film seal, and analyzed the parameters of inclined elliptical micro pore. The research provides a model reference for the further research of flexible support structure [14,15]. Sun et al. discussed the effect of operating parameters of T-groove CGFS on gas sealing performance and steady-state characteristics under the action of single flow field and analyzed the effect of groove parameters on the pressure distribution, gas film stiffness, and leakage. The research optimized the T-groove parameters and obtained the best T-groove structure under certain working conditions and provided basic gas film model data for the study of this manuscript [16,17]. However, most researchers have not analyzed the structural performance of flexible support. As the main component of CGFS, the flexible support structure determines the ability of CGFS to overcome radial runout and the dynamic stability of the system. In this paper, a straight-groove CGFS with wave foil structure and flexible support is studied. The fluid-structure coupling analysis method is used to study the flow field characteristics of the CGFS and the impact of the structural parameters and the flexible support material parameters on the performance of the support structure.

2. Model

2.1. Physical Model

There is eccentricity between the moving ring and the floating ring. When the moving ring rotates at high speed, the hydrodynamic effect is formed between the two rings, and the gas film with sufficient stiffness is produced, which separates the two rings from each other in the sealing process and keep dynamic process in balance. The non-contact state between the flat foil and the moving ring can avoid wear and friction and lead to better lubrication effect.

The CGFS system consists of flexible wave foil, floating ring (flat foil), moving ring, and rotating shaft, while the flexible supporting structure mainly contains the flexible wave foil and flat foil, as shown in Figure 1.When the moving ring rotates with the rotating shaft at high speed, gas is pumped into the straight groove. With the dynamic groove and eccentric structure, the gas is compressed in the convergence area, which generates high pressure and hence a layer of micron scale gas film between the floating ring and the moving ring. Therefore, the dynamic groove and the convergent gap formed by the eccentric installation of moving ring and floating ring are the main causes for the hydrodynamic effect of CGFS.

The radial vibration generated by the rotating shaft is transmitted to the floating ring in the form of film compression force. The flexible wave foil installed at the bottom of the floating ring can cushion the radial runout caused by precession of rotor, and hence to

prevent the seal pair from rubbing, friction heating, and "shaft holding". Therefore, the failure of the seal can be prevented, and the reliability of the seal is improved.

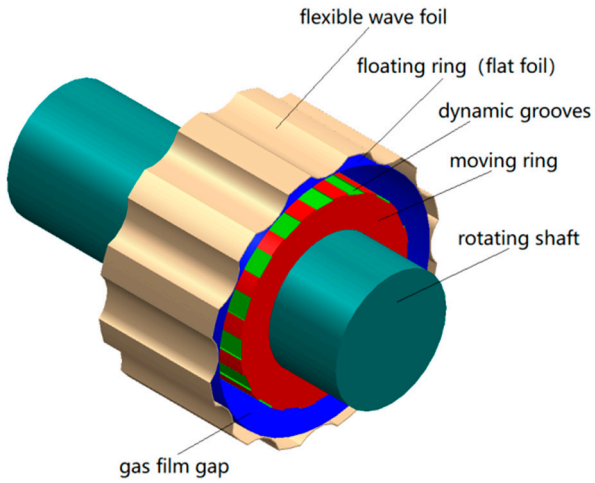

Figure 1. Schematic diagram of flexible support cylindrical gas film straight groove seal structure.

2.2. Mathematical Model

The general principle of CGFS for the high-speed flexible rotor system of aviation gas turbine is based on the physical model of radial bearing with circular precession. As shown in Figure 2, when the rotor rotates at speed ω_j, the center O_j of rotor journal has a precession extrusion velocity $e\Omega$, where Ω is the instantaneous precession angular velocity, and under the steady synchronous condition, $\Omega = \omega_j$. There is also radial extrusion velocity $\dot{e}$ (e is eccentricity). Furthermore, the stator inner hole can rotate at the angular velocity ω_b, and under such a condition, the trajectory of the rotor center O_j around the stator hole O_b will be unsteady with non-circular precession. Only when e is a constant and $\dot{e} = 0$ does the trajectory of O_j have circular precession.

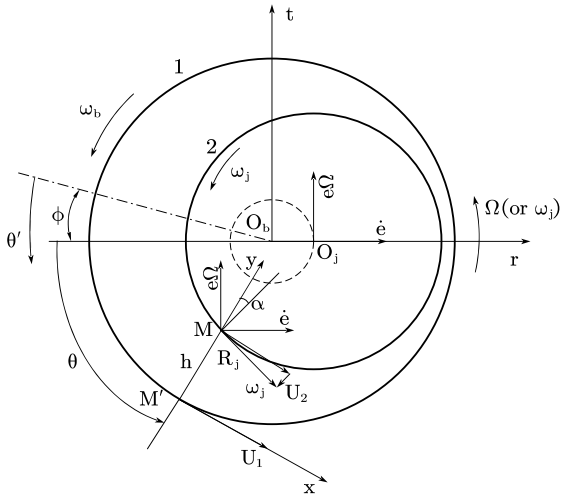

Figure 2. Rotating coordinate system and bearing motion.

In the rotating coordinate system (r, t, z) shown in the Figure 2, the Reynolds equation of fluid film lubrication for rotor journal under unsteady precession is established.

$$\frac{1}{R_j^2}\frac{\partial}{\partial\theta}\left(\frac{\rho h^3}{\eta}\frac{\partial p}{\partial\theta}\right)+\frac{\partial}{\partial z}\left(\frac{\rho h^3}{\eta}\frac{\partial p}{\partial z}\right)=6(U_1+U_2)\frac{\partial(\rho h)}{R_j\partial\theta}+12\frac{\partial(\rho h)}{\partial t} \quad (1)$$

When the cylindrical gas film is working under typical operating conditions, we have the Equations (2) and (3):

$$U_1 \approx R_\mathrm{j}\omega_b \tag{2}$$

$$U_2 \approx R_\mathrm{j}\omega_\mathrm{j} \tag{3}$$

With the gas state equation given in Equation (4), together with Equations (1)–(3),

$$\rho = \frac{M}{RT}\mathrm{p} \tag{4}$$

Equation (5) can be obtained,

$$\frac{1}{R^2}\frac{\partial}{\partial\theta}\left(\frac{ph^3}{\eta T}\frac{\partial p}{\partial\theta}\right) + \frac{\partial}{\partial z}\left(\frac{ph^3}{\eta T}\frac{\partial p}{\partial z}\right) = 6\omega\frac{\partial}{\partial\theta}\left(\frac{ph}{T}\right) + 12\frac{\partial}{\partial t}\left(\frac{ph}{T}\right) \tag{5}$$

where R is the external radius of the moving ring (unit: m), θ is the circular coordinate (unit: rad), p is the lubrication film pressure (unit: Pa), his the film thickness (unit: m), η is the viscosity of lubricating gas (unit: $N{\cdot}\mathrm{s}/\mathrm{m}^2$), T is the temperature of lubricating gas (unit: °C), z is the axial coordinate (unit: m), ω is the angular velocity of rotor(unit: rad/s), t is the running time (unit: s). Let us define,

$$\overline{\mathrm{z}} = \frac{\mathrm{z}}{L}, \overline{\mathrm{h}} = \frac{\mathrm{h}}{C}, \overline{\mathrm{p}} = \frac{\mathrm{p}}{p_a}, \overline{\mathrm{T}} = \frac{T}{T_0}, \overline{\eta} = \frac{\eta}{\eta_0}, \overline{\mathrm{t}} = \mathrm{vt} \tag{6}$$

Furthermore, the dimensionless Reynolds equation shown in Equation (7) can be obtained by substituting Equation (6) into Equation (5),

$$\frac{\partial}{\partial\theta}\left(\frac{\overline{\mathrm{p}}\overline{\mathrm{h}}^3}{\overline{\eta}\,\overline{T}}\frac{\partial\overline{p}}{\partial\theta}\right) + \frac{R^2}{L^2}\left(\frac{\overline{\mathrm{p}}\overline{\mathrm{h}}^3}{\overline{\eta}\,\overline{T}}\frac{\partial\overline{p}}{\partial\overline{\mathrm{z}}}\right) = \Lambda_\mathrm{x}\frac{\partial}{\partial\theta}\left(\frac{\overline{\mathrm{p}}\overline{\mathrm{h}}}{\overline{T}}\right) + 2\Upsilon\Lambda_\mathrm{x}\frac{\partial}{\partial\overline{\mathrm{t}}}\left(\frac{\overline{\mathrm{p}}\overline{\mathrm{h}}}{\overline{T}}\right) \tag{7}$$

where Λ_x is the compressible coefficient and Υ is the disturbance ratio with definitions given as follows,

$$\Lambda_\mathrm{x} = \frac{6\omega\eta_0 R^2}{\mathrm{p_a}C^2} \tag{8}$$

$$\Upsilon = \frac{\mathrm{v}}{\omega} \tag{9}$$

2.3. Calculation of Gas Film Steady Sealing Characteristic Parameters

2.3.1. Film Buoyancy Lift

The film buoyancy lift is a force from sealing gas acting on the moving ring and static ring under the hydrodynamic effect. When the film buoyancy lift reaches a certain value, the floating ring and the moving ring are separated, and the dynamic balance appears. At this time, the film buoyancy lift and the supporting force of the flexible support balance each other, and a non-contact gas friction is formed. The formula for calculating the film buoyancy lift is obtained by integrating the distribution of pressure field of cylindrical gas film.

$$\begin{cases} F_\mathrm{r} = \int_0^1\int_0^{2\pi}(\mathrm{p}-\mathrm{p_a})R_\mathrm{j}\cos\theta\,\mathrm{d}\theta\mathrm{d}z \\ F_\mathrm{t} = \int_0^1\int_0^{2\pi}(\mathrm{p}-\mathrm{p_a})R_\mathrm{j}\sin\theta\,\mathrm{d}\theta\mathrm{d}z \\ F_\mathrm{g} = \sqrt{F_\mathrm{t}^2 + F_\mathrm{r}^2} \end{cases} \tag{10}$$

Dimensionless form of Equation (10) is shown in Equation (11),

$$\overline{F} = \frac{\mathrm{F}}{P_{\mathrm{a}} R_{\mathrm{j}} L} \tag{11}$$

R_j is the radius of moving ring (unit: m), F_{r} is the radialfilm buoyancy lift (unit: N), F_{t} is the tangential film buoyancy lift (unit: N),F is the resultant film buoyancy lift (unit: N), p is the film pressure (unit: Pa), P_a is the ambient pressure (unit: Pa), and θ is the circumferential angle (unit: degree).

2.3.2. Leakage

The leakage is an important indicator to judge whether the seal is invalid. The more leakage, the easier the seal will fail. The leakage can be calculated using Equation (12),

$$Q = 2\int_0^{2\pi} \rho \left(-\frac{\mathrm{h}^3}{12\eta} \frac{\partial \mathrm{p}}{\partial \mathrm{z}} \right) R_{\mathrm{j}} \mathrm{d}\theta \mathrm{dz} \tag{12}$$

Its dimensionless form is shown in Equation (13),

$$\overline{Q} = -24 \frac{\eta RTL}{\mathrm{p}_{\mathrm{a}}^2 \mathrm{c}^3 R_{\mathrm{j}}} Q \tag{13}$$

where h is the average film thickness (unit: m), Q is the leakage (unit: kg/s), ρ is the gas density (unit: kg/m^3), η is the dynamic viscosity of gas (unit: Pa·s), R_{j} is the radius of the moving ring (unit: m), and P is the gas film pressure (unit: Pa).

2.3.3. Gas Film Stiffness

Gas film stiffness is the ratio between the increment of film buoyancy lift and the increment of film thickness, which is a crucial indicator reflecting the gas film bearing capacity. The larger the gas film stiffness is, the stronger the gas film bearing capacity is, and the better gas film sealing ability is. The stiffness calculation formula is shown in Equation (14):

$$K_{\mathrm{zz}} = -\left.\frac{\partial F_{\mathrm{z}}}{\partial \mathrm{h}}\right|_{\mathrm{h0}} = -\frac{F_2 - F_1}{\mathrm{h}_2 - \mathrm{h}_1} \tag{14}$$

Its dimensionless form is shown in Equation (15):

$$K_{\mathrm{zz}} = -\frac{\overline{F_2} - \overline{F_1}}{\overline{\mathrm{H}_2} - \overline{\mathrm{H}_1}} \tag{15}$$

where K_{zz} is the radial gas film stiffness (N/m), F_1 is the film buoyancy lift when the film thickness is h_1 (N), F_2 is the film buoyancy lift when the film thickness is h_2 (N), h_1 is the average film thickness at the start point (m), and h_2 is the average film thickness at the end point (m).

3. Model Parameters

3.1. Parameters of Flexible Supporting Structure

The flexible supporting structure consists of flexible wave foil and floating ring. The flexible wave foil is mainly used to cushion the deviation of the rotating shaft in the process of gas film movement, so as to prevent the failure caused by the collision between the moving ring and the floating ring. The local model of wave foil is shown in Figure 3, and the structural parameters and operating parameters type values are provided in Table 1.

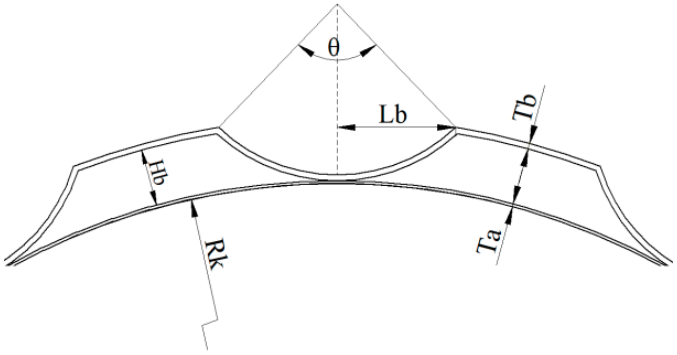

Figure 3. Schematic diagram of wave foil structure.

Table 1. Definition of flexible support cylindrical gas film seal (unit in given the bracket).

Parameter Type	Parameters	Value
Structural parameter	Floating ring radius Rk (mm)	25.02
	Moving ring radius Rj (mm)	25
	Average film thickness h(mm)	0.02
	Eccentricity ε	0.6
	Ring length L(mm)	52
	Groove length L1 (mm)	25
	Groove depth H (μm)	5
	Number of groove N	16
	Floating ring thickness Ta (mm)	0.1
	Wave foil thickness Tb (mm)	0.102
	Wave foil height Hb (mm)	0.588
	Wave foil ripple half Chord length Lb (mm)	1.88
Operating parameter	Rotational Speed n ($r \cdot min^{-1}$)	13,000
	Inlet pressure Pi (MPa)	0.3
	Outlet pressure Po (MPa)	0.1
	Temperature T (°C)	26.85
	Gas viscosity v (Pa·s)	1.79×10^{-5}

3.2. Basic Assumptions

3.2.1. Basic Assumption of Flow Field

The operating conditions of cylindrical micro groove gas film seal have the flowing assumptions: Firstly, the gas is an ideal gas, which is uniform and continuous and obeys Newton's viscosity principle. Secondly, the impact of gas volume force and inertia force on the flow field is negligible. Thirdly, the temperature and viscosity in the flow field remain constant. Fourthly, there is no relative slip between the fluid and the shaft, and between the fluid and the floating ring. Lastly, there is no vibration in the gas film. This paper focuses on the law of influence of operating parameters and sealing structure parameters on the flow field characteristics, and therefore, the selection of uniform and continuous ideal gas has negligible impact on the research results.

3.2.2. Basic Assumptions of Wave Foil Structure Bending

The shell theory is used to solve the stress and deformations of wave foil and flat foil with the following assumptions. Firstly, there is no shear force in the foil and no extrusion or stretching between the layers in the horizontal direction. Secondly, when the foil is loaded perpendicular to the middle plane, there is no displacement between the points parallel to the wave foil. Thirdly, there is no friction between the foil and journal, and no friction between the wave foil and floating ring. Lastly, the axial stiffness variation of wave foil is negligible.

3.3. Modelling and Meshing

In a flexible support CGFS structure, because of the eccentricity, the film thickness between the moving ring and the floating ring is not uniformly distributed along the circumference. Therefore, the quality and quantity of grids will directly affect the accuracy of the results and computation time of the analyses. In the paper, ANSA software is used to mesh the fluid region and the flexible support solid region. The schematic diagrams of the meshes are shown in Figure 4.

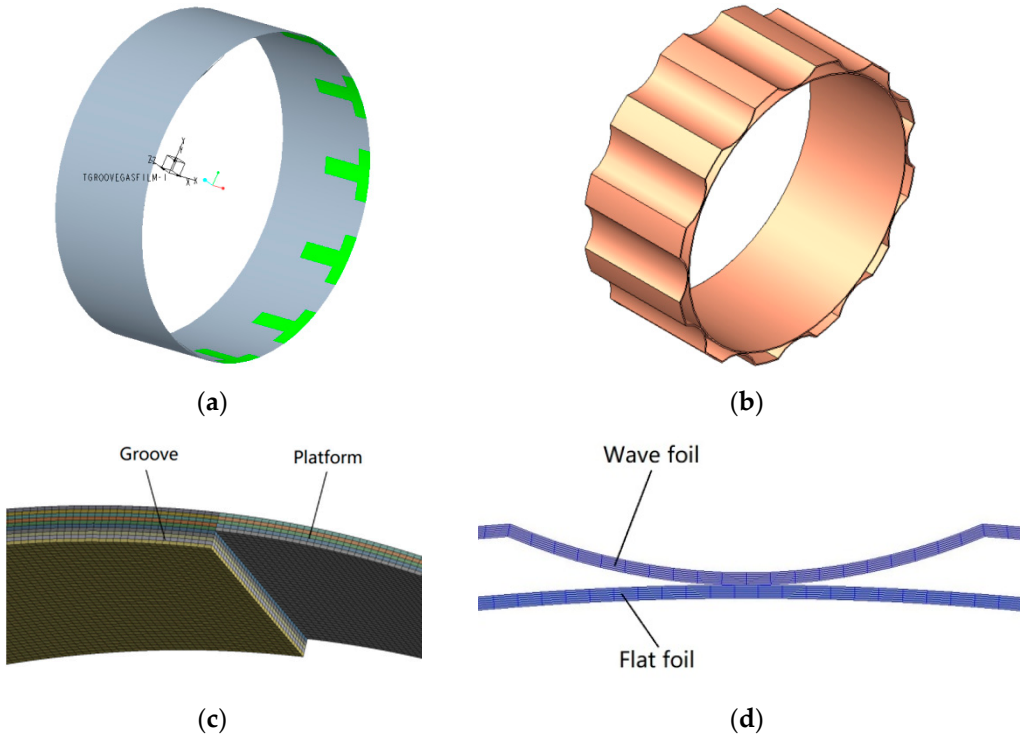

Figure 4. Model and grid. (**a**) Gas film model; (**b**) flexible support model; (**c**) gas film local grid; (**d**) wave foil local grid.

3.4. Boundary Conditions and Solver Setting

The inlet boundary is set as the pressure inlet, Pi = 0.3 MPa, and the outlet boundary is set as the pressure outlet, Po = 0.1 MPa. The inlet temperature is set to 26.85 °C. The inner wall surface is set as the rotating surface, and the speed is 13,000 r/min. The outer wall is set as the stationary surface. The software solver is set to SIMPLE pressure correction method.

4. Analysis of Flow Field Characteristics

4.1. Effect of Operating Parameters on Sealing Ability

This section mainly studies the impacts of rotor rotational speed and inlet and outlet pressure difference on the leakage, gas film stiffness, and sealing ability.

4.1.1. The Impacts of Rotational Speed

The rotational speed range of rotor is set to [7000, 17,000] rpm, and the other parameters are listed in Table 1. It can be seen from Figure 5 that when the speed increases from 7000 rpm to 17,000 rpm, the leakage decreases gradually, and the gas film stiffness increases gradually. This is because when the rotor speed increases, the motion of seal gas in the rotating flow field intensifies, the friction torque between gas molecules increases, and the hydrodynamic effect increases. So, the bearing capacity per unit gas film thickness increases correspondingly, and the gas film stiffness increases. Therefore, the sealing performance improves. The change rate of leakage is about 0.11%, and the change rate of stiffness is

about 1.7%. This indicates that when the rotating speed is over 7000 rpm, the increase of rotating speed has relatively small impact on the sealing performance. From the point of view of the applicability of the seal, the result shows that this seal structure is suitable for a wide range of speed and can be used widely.

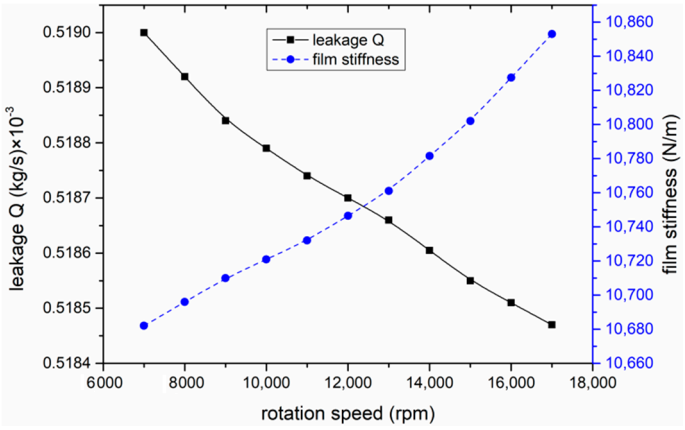

Figure 5. Effect of rotational speed on leakage and gas film stiffness.

4.1.2. The Impact of Pressure Difference

The rotational speed is set to n = 13,000 rpm and keep the groove parameters and outlet pressure unchanged. Set the inlet pressure range to [0.2, 0.5] MPa, and other parameters are shown in Table 1.Therefore, the pressure difference is [0.1, 0.4] MPa. The impacts of pressure difference on leakage and gas film stiffness are shown in Figure 6, and the result shows that the leakage rises linearly when the pressure difference increases. This is because in the gas film flow field, the gas viscosity is low, so when the pressure difference increases, the pumping effect of the fluid is enhanced, and the fluid velocity along the axis direction rises, resulting in the rise of the leakage. When the inlet pressure rises from 0.2 MPa to 0.5 MPa, the gas film stiffness increases by 3.8%, and the increment of leakage is about 387%. The main reason is that when the inlet pressure increases, the overall pressure in the clearance flow field increases, which leads to a significant increase of the end discharge of the outlet. Meanwhile the increase of the pressure will increase the hydrodynamic effect and increase the gas film buoyancy lift on the unit film thickness. The result is shown in Figure 6.

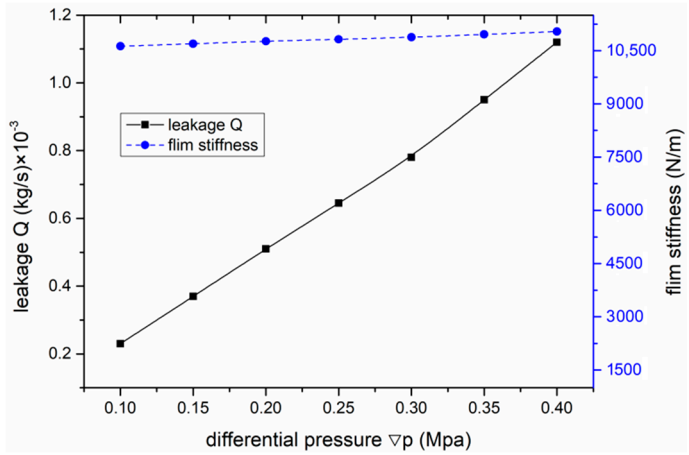

Figure 6. Impactof pressure difference on leakage and gas film stiffness.

4.2. Impacts of Structural Parameters on Sealing Performance

In order to study the impacts of structural parameters, such as eccentricity, groove number, and groove depth, on sealing performance, the following conditions are assumed: the temperature is 26.85 °C, the rotational speed is 13,000 rpm, the inlet pressure is 0.3 MPa, and the outlet pressure is 0.1 MPa.

4.2.1. Impact of Eccentricity

Figure 7 shows the impact of eccentricity on leakage, film buoyancy lift, and film stiffness. The leakage and film buoyancy lift increase when the eccentricity increases, and the reason is that when the eccentricity increases, the thickness at the maximum gap position becomes larger and the minimum film thickness decreases, which enhances the local wedge effect and hydrodynamic effect. However, the position of maximum film thickness becomes opposite, which leads to the increase of film buoyancy life. Under the composite influence, the increase of eccentricity can promote the film buoyancy lift, but the effect is relatively weak. The gas film stiffness reduces with the increase of eccentricity, this is because when the eccentricity grows, the film buoyancy lift increases slightly. However, the ratio of the increment of film buoyancy lift to the eccentricity increment is decreasing.

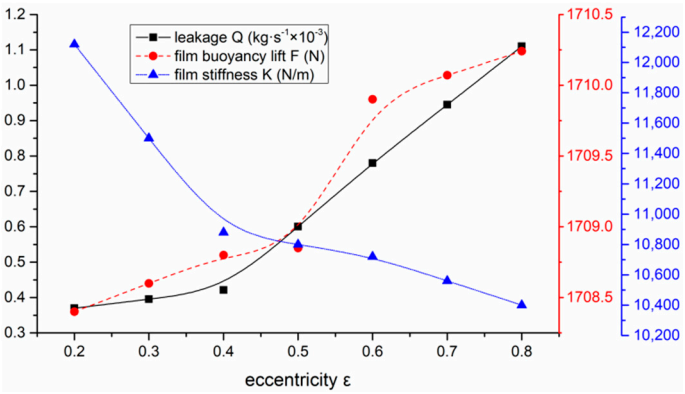

Figure 7. Impact of eccentricity on leakage, film buoyancy lift and gas film stiffness.

4.2.2. Impact of Number of Grooves

Figure 8 shows the impact of number of grooves on the leakage, film buoyancy lift, and gas film stiffness. The leakage grows with more grooves, since the axial outflow of gas film increases with the bigger groove area. Results show that film buoyancy lift increases with the number of grooves increases. This phenomenon can be explained as follows. When the number of grooves increases, the wedge effect increases, and the hydrodynamic effect increases, which leads to the increase of film buoyancy lift. On the other hand, the film stiffness decreases with the increase of the number of grooves. The eccentricity increment is more than the film buoyancy lift increment. Therefore, the film stiffness decreases continuously.

4.2.3. Impact of Groove Depth

Figure 9 shows the impact of groove depth on leakage, film buoyancy lift, and gas film stiffness. When the groove depth changes from 5 μm to 20 μm, the leakage increases steadily. This is because there is more gas pumped into the gap, which leads to more gas flow out along the axial direction, and the leakage becomes larger. The reason for the increase of film buoyancy lift is that when the groove depth increases, the hydrodynamic effect is increasing in the dam area, which leads to the increase of film buoyancy lift. The gas film stiffness increases from 10,770 N/m to 278,325 N/m with the increase of groove depth. This is because although the gas film thickness increases, the variation of film buoyancy lift becomes greater, which leads to the rise of gas film stiffness.

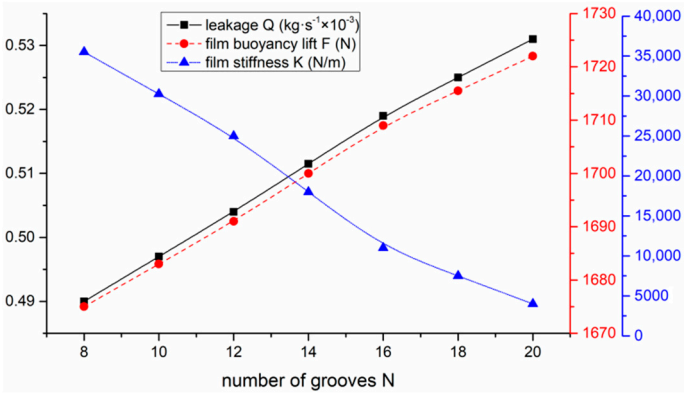

Figure 8. Impact of number of grooves on leakage, film buoyancy lift, and gas film stiffness.

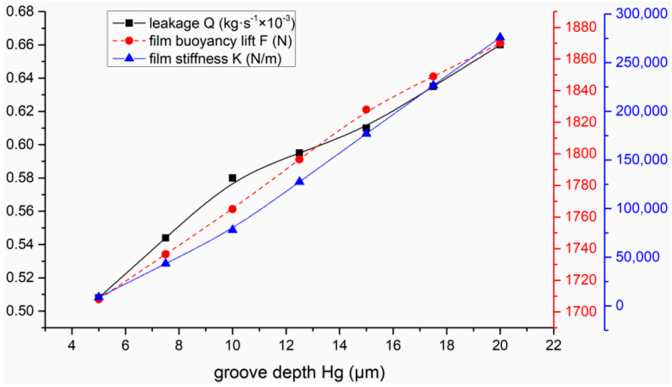

Figure 9. Effect of groove depth on leakage, film buoyancy lift, and gas film stiffness.

4.2.4. Impact of Groove Length

Figure 10 shows the impact of groove length on leakage, film buoyancy lift, and gas film stiffness. As the length of groove increases, the volume of gas passage along the axis increases. Therefore, when the sealing system is running, the gas leakage increases slightly. When the groove length is less than 30 mm, the increase of groove length leads to the increase of hydrodynamic effect, and the film buoyancy lift increases slightly. However, when the groove length is greater than 30 mm, the fluid flow channel in the gap becomes longer, which weakens the hydrodynamic effect, and the film buoyancy lift starts to decrease. The film stiffness declines significantly as the increase of groove length, because the eccentricity increment increases significantly while the film buoyancy lift only increases slightly, which results in a decrease of gas film stiffness.

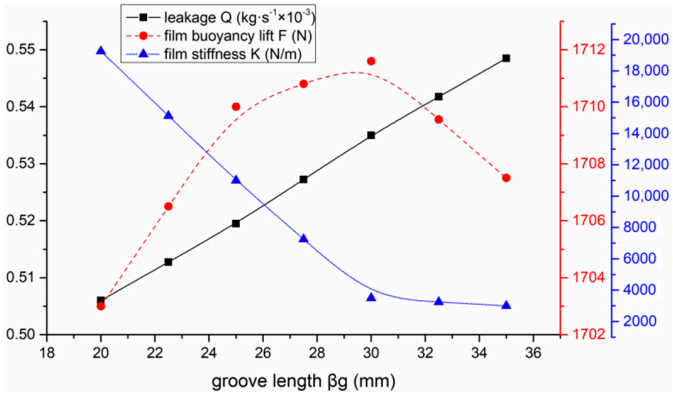

Figure 10. Impact of groove length on leakage, film buoyancy lift, and gas film stiffness.

5. Fluid-Structure Coupling Analysis of Flexible Support Performance

When the rotor rotates with low speed, the hydrodynamic effect is weak, and the gas film is unstable. The fluctuating load of rotor structure is mainly transformed into the deformation energy of wave foil. A proper thickness of the gas film should be ensured to prevent the rotor contacting the wave foil directly in order to avoid potential wearing. When the moving ring is at high speed, the film stiffness is sufficient to support the rotor, but the whirling energy generated by the radial runout of rotor needs to be absorbed by elastic deformation of foil structure to ensure the stability of the operation. Therefore, studying the factors that affect the performance of flexible supporting structures is of great importance in engineering application for better understanding the CGFS performance and its dynamic mechanical characteristics.

5.1. Average Gas Film Thickness

Figure 11 shows the impact of film thickness on the maximum equivalent stress and the average equivalent stress of the flexible support. As the film thickness changes from 10 μm to 15 μm, the maximum equivalent stress of the flexible support decreases from 102.96 MPa to 69.76 MPa, and the average equivalent stress also decreases obviously. This is because when the average film thickness increases, the wedge effect weakens, the hydrodynamic effect decreases, and the maximum equivalent stress on the flexible support also decreases. When the film thickness is larger than 15 μm, the hydrodynamic effect reduces to a stable level. At this time, the effect of the flow field on the flexible support structure is reduced, and the equivalent stress of the flexible support structure is slightly changed.

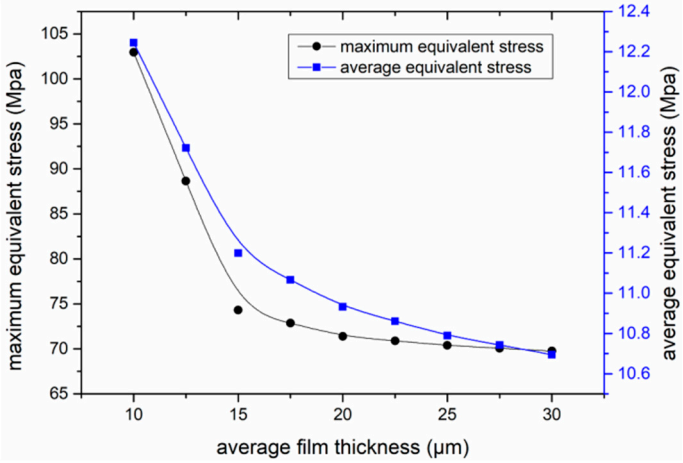

Figure 11. The impact of film thickness on the maximum equivalent stress and the average equivalent stress of the flexible support.

5.2. Eccentricity

Figure 12 shows the results of the equivalent stress while eccentricity is increased from 0.2 to 0.8.As shown in Figure 12, when the eccentricity varies from 0.2 to 0.6, the equivalent stress rises slightly. When the eccentricity is 0.2, the maximum equivalent stress is 68.9 MPa and the maximum deformation is 8.60×10^{-3} mm. When the eccentricity is 0.6, the maximum equivalent stress is 71.40 MPa, and the maximum deformation is 8.82×10^{-3} mm. These results indicate that when the eccentricity changes from 0.2 to 0.6, the force acting on the flexible support increases gradually. This is because when the eccentricity increases, both the minimum film thickness and wedge-shaped gap become smaller, and the hydrodynamic effect is enhanced. Meanwhile, the buoyancy lift of clearance flow field increases, and the force acting on the interface of floating ring becomes larger. However, when the eccentricity is more than 0.6, the deformation and equivalent stress tend to be stable, because when the eccentricity exceeds 0.6, the film buoyancy lift

tends to be stable, and the force acting on the floating ring tends to be stable. The results are illustrated in Figure 7.

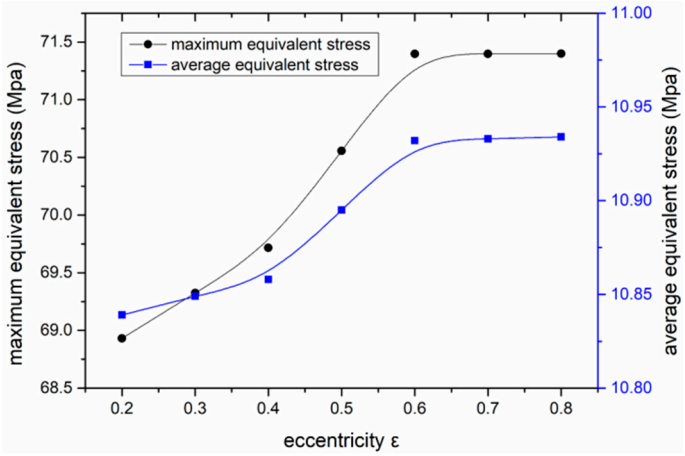

Figure 12. Impact of the eccentricity on the average and maximum equivalent stresses.

5.3. Number of Wave Foils

Figure 13 shows the variation curve of equivalent stress with the number of flexible supporting wave foils. The results show that when the number of wave foils is 8, the maximum equivalent stress is 81.9 MPa, and then the maximum equivalent stress decreases with the increase of number of the wave foils. When the number is 14, the maximum equivalent stress reaches the minimum value of 67.4 MPa. After that, with the increase of the number of wave foils, the maximum equivalent stress gradually increases with fluctuation. When the number is 30, the maximum equivalent stress is 78.84 MPa. On the other hand, when the number of wave foils increases from 8 to 30, the average value of equivalent stress decreases steadily. This is because with the increase of number of wave foils, the number of inner convex structures along the circumferential direction on the wave foils increases, and the overall bending strength of the wave foils increases. Therefore, the deformation of the flexible support decreases and the equivalent stress decreases. However, when the number of wave foils increases, the deformation of local wave foil increases slightly.

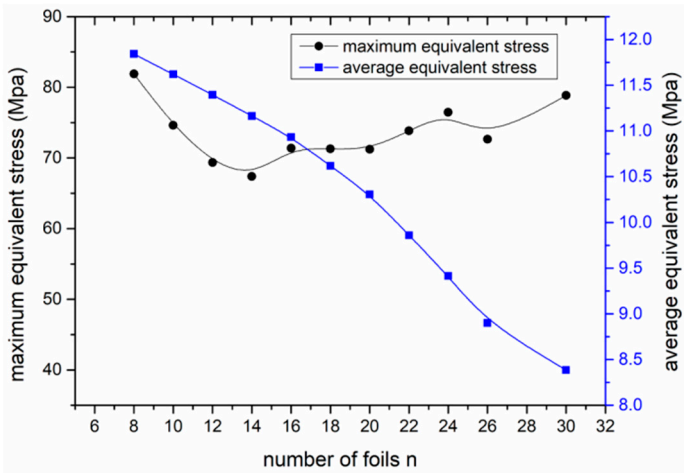

Figure 13. Impact of number of foil numbers on equivalent stress changing.

To sum up, when selecting the number of wave foils based on their deformation and the equivalent stress, it can be neither too big nor too small. When the number of wave foils is too small, the deformation is large, the support stiffness is small, and the shaft is

prone to instability. When the number of wave foils is too big, the deformation is small, the support stiffness is large, and the radial runout of the shaft cannot be buffered, which can lead to failure of the seal. Based on the results discussed in this paper, the recommended number of wave foils is 14.

6. Conclusions

In this paper, the effects of operating and structural parameters of the straight-groove seal on the hydrodynamic pressure, leakage, and film stiffness are studied. The effects of gas film thickness, eccentricity, and the wave foils number on the equivalent stress of flexible support are also analyzed. From the results, the following conclusions can be obtained.

(1) When the rotor speed increases, the sealing performance improves slightly. From the perspective of the sealing applicability, it shows that the sealing parameters used in this paper are suitable for working conditions with high rotational speed. Since the increase of pressure difference leads to increase of leakage, this counteracts the hydrodynamic effect. Therefore, although the gas film stiffness increases, the increase is relatively small.

(2) As the eccentricity increases, the film thickness increases at the largest film gap but decreases at the minimum film gap. With the combined effects, the leakage increases significantly, the film buoyancy lift increases slightly, and the gas film stiffness decreases. As the number of grooves increases, the wedge and hydrodynamic effects are enhanced, the leakage and film buoyancy increase, and the film stiffness decrease continuously. When the groove depth increases, the wedge effect increases slightly, and the film stiffness increases significantly. When the groove length increases, the film buoyancy lift increases first and then decreases, the leakage increases, and the gas film stiffness decreases significantly.

(3) As the average film thickness increases, the hydrodynamic effect declines and the force acting on the flexible support decreases, so the average equivalent stress of the flexible support also decreases. When the film thickness is bigger than 15 μm, the equivalent stress of the flexible support tends to be stable.

(4) As the eccentricity increases, the wedge-shaped gap between the moving ring and floating ring becomes smaller, the hydrodynamic effect is enhanced, the force of gas film acting on the flexible support in the flow field increases, and the equivalent stress increases accordingly, when the eccentricity is bigger than 0.6, the equivalent stress stabilizes gradually.

(5) As the number of wave foils increases, the effective resistance area of wave foils against the pressure of gas film becomes larger, so the deformation of wave foil and the average equivalent stress decrease. Therefore, if the number of wave foils is too big, the bearing capacity and ability to resist deformation of flexible support structure is strengthened, but the radial displacement of rotor cannot be buffered effectively. Therefore, the selection of the number of wave foils should consider both the support rigidity and the ability to buffer the radial displacement effectively.

7. Patents

The CGFS structure involved in this manuscript is designed by the authors. It has been applied for a patent in China and has been authorized. The patent name is: A double acting flexible support dry gas sealing device with end face and cylinder surface combination. The patent number is ZL201822008358.5.

Author Contributions: Conceptualization, J.S.; data analyses, Y.L.; investigation, J.S., M.L., T.L. and X.H.; methodology, M.L. and X.H.; resources, Z.X. and J.W.; software, Z.X., Y.L. and J.W.; writing—original draft, J.S., Z.X. and T.L.; writing—review and editing, J.S., M.L. and X.H. All authors have read and agreed to the published version of the manuscript.

Funding: This research was funded by the National Natural Science Foundation of China, grant number 51765024. The research was also funded by the Opening fund of State Key Laboratory of Nonlinear Mechanics.

Institutional Review Board Statement: Not applicable.

Informed Consent Statement: Not applicable.

Data Availability Statement: The data presented in this study are available on reasonable request from the corresponding author.

Acknowledgments: The authors greatly appreciate assistance from Xiaolei Song and Junjie Lei in data modeling.

Conflicts of Interest: The authors declare no conflict of interest.

References

1. Shen, H.; Zheng, T.; Chen, Y. Improvement of aero-engine sealing technology. *Gas Turbine Exp. Res.* **2011**, *4*, 51–55.
2. Steinetz, B.M.; Hendricks, R.C. Engine seal technology requirements to meet NASA's Advanced Subsonic Technology program goals. *J. Propuls. Power* **1996**, *12*, 786–793. [CrossRef]
3. Ma, G.; Sun, X.; Luo, X.; He, J. Numerical simulation analysis of steady-state properties of gas face and cylinder film seal. *J. Beijing Univ. Aeronaut. Astronaut.* **2014**, *4*, 439–443.
4. Su, Z.; Liu, M. CFD numerical simulation of cylindrical gas film seal properties. *Lubr. Eng.* **2016**, *9*, 49–53.
5. Ma, G.; Shen, X. Research progress and analysis of advanced gas film sealing technology. *Aviat. Manuf. Technol.* **2009**, *3*, 58–61.
6. Chen, T.; Liu, M. Research progress and development trend of cylindrical gas film seal. *New Technol. New Process* **2014**, *6*, 78–81.
7. Sun, J.; Liu, M.; Li, Y.; Su, Z.; Kang, Y. Analysis on steady fluid dynamics of cylindrical gas seal by CFD. *Drain. Irrig. Mach.* **2017**, *11*, 968–974.
8. Sedy, J. A new self-aligning mechanism for the spiral-groove gas seal stability. *Lubr. Eng.* **1980**, *36*, 592–598.
9. Song, L. Current development of dry gas seal used with large diameter shaft at home and abroad and application in china. *Process Equip. Pip.* **2016**, *1*, 39–42.
10. Ma, G.; Xu, G.; Shen, X. Design and analysis for spiral grooved cylindrical gas seal structural parameter. *Lubr. Eng.* **2007**, *4*, 127–130.
11. Ma, G.; He, J.; Li, X.; Shen, X. Numerical calculation of dynamic characteristic coefficient of gas film seal. *J. Mech. Eng.* **2013**, *49*, 55–62. [CrossRef]
12. Ma, G.; Li, X.; Shen, X.; Hu, G. Analysis of performance and interface structure of cylinder gas film seal. *J. Aerosp. Power* **2011**, *11*, 2610–2616.
13. Ma, G.; He, J.; Sun, X.; Shen, X. Nonlinear numerical simulation for dynamic characteristic of gas cylinder film seal. *J. Aerosp. Power* **2014**, *1*, 1–8.
14. Ding, X.; He, Z.; Zhang, W.; Lu, J.; Miao, C. Steady state approximate calculation of micro scale flow field in cylindrical spiral groove dry gas seal. *Chin. J. Appl. Mech.* **2018**, *1*, 99–105.
15. Ding, X.; He, Z.; Zhang, W.; Lu, J.; Miao, C. Parameters analysis of steady micro-scale flow of cylindrical spiral groove dry gas seal. *J. Chem. Ind. Eng.* **2018**, *4*, 1537–1546.
16. Sun, J.; Liu, M.; Xu, Z.; Liao, T. Research on operating parameters of T-groove cylindrical gas film seal based on computational fluid dynamics. *Adv. Compos. Lett.* **2019**, *28*, 1–7. [CrossRef]
17. Sun, J.; Liu, M.; Xu, Z.; Liao, T.; Hu, X. Effect of T-groove Parameters on Steady-State Characteristics of Cylindrical Gas Seal. In Proceedings of the Advanced Manufacturing and Automation IX (IWAMA 2019), Plymouth, UK, 21–22 November 2019; Springer: Singapore, 2020; pp. 427–433.